Journal of Power Sources 242 (2013) 672–676

Contents lists available at SciVerse ScienceDirect

Journal of Power Sources

journal homepage: www.elsevier.com/locate/jpowsour

Short communication

Fabrication and performance evaluation of an in-membrane micro-fuel cell

Ayokunle Omosebi*, Ronald S. Besser

Department of Chemical Engineering and Materials Science, Stevens Institute of Technology, Hoboken, NJ 07030, USA

HIGHLIGHTS

- Fabrication of an in-membrane μFC via e-beam lithography, dry etching and electrode patterning.
- Investigation of pattern deformation under compressive load.
- Fabrication of testing fixture for in-membrane μFC via a hot-pressing procedure.
- Performance comparison of sputtered Pt and dispersed Pt/C thin film catalysts in a planar μFC architecture.

ARTICLE INFO

Article history:
Received 21 December 2012
Received in revised form
30 April 2013
Accepted 27 May 2013
Available online 6 June 2013

Keywords:
Micro-fuel cell
Planar fuel cell
Electron beam lithography
Nafion patterning
PEMFC

ABSTRACT

A new approach to fabricating planar micro-fuel cells with flow channels and catalyst layers fully integrated into the Nafion membrane is presented. The microfabrication approach leverages the use of electron beam lithography for pattern creation, dry etching for pattern transfer and aspect ratio manipulation, and masking for selective electro-catalyst layer deposition. Sputtered Pt and conventional Pt/C served as catalyst layers for the fabricated cells which were tested under humid and dry conditions. The sputtered cell had the best overall performance. The maximum power densities were respectively 11.2 and 20.8 mW cm^{-2} for the dry and humidified conventional catalyst based cells, and 3.0 and 22.1 mW cm^{-2} for the sputtered Pt cells. Based on these results, the authors conclude that the observed performance is limited by ohmic polarization.

1. Introduction

Advances in microfabrication technology, miniaturization and rapid prototyping have led to the continued growth of the electronics industry over the past five decades. As a result, cheaper, faster and more efficient electronic and wireless devices are continuously being deployed [1–3]. These devices currently rely on batteries as a power source, but the need for constant replacement and recharging, interrupted operation, disposal issues, and increasing power requirements has prompted the development of new power sources [1–4]. Micro-fuel cells (μFCs) are being considered as viable alternatives due to their high energy density and environmental friendliness [3–7].

Fuel cells produce DC electricity directly from the stored chemical potential in their fuel and oxidant input. For μFCs, their power density ranges from several μWs cm^{-2} to hundreds of mWs cm^{-2} [1,2]. Categorically, μFCs can differ by fuel–oxidant combination, ionic media variation, and the degree to which microfabrication is employed for flow channel and electrode design [1,2]. The most common architecture is a set of microfabricated flow channels and current collector sandwiching a membrane electrode assembly (MEA) [2]. At the moment, material selection for microfabricated μFCs is limited to established microfabrication materials like silicon, poly methyl methacrylate (PMMA) [7,8], and polydimethylsiloxane (PDMS) [9]. Fuel cells are typically stacked in order to increase power density which leads to bulkier devices. New planar type μFC architectures have recently emerged where proton conduction is in-plane versus the traditional through-plane orientation [10–14]. These planar μFCs can facilitate the deployment of thinner and reduced form factor power sources. Despite continued improvement, several issues including gas crossover, sealing, and high membrane resistance continue to limit the μFC.

Distinct from previously fabricated in-plane μFC by other researchers, in this work we present a novel μFC design where the

* Corresponding author. Tel.: +1 201 216 5523; fax: +1 201 216 8306.
E-mail address: aomosebi@stevens.edu (A. Omosebi).

0378-7753/$ – see front matter © 2013 Elsevier B.V. All rights reserved.
http://dx.doi.org/10.1016/j.jpowsour.2013.05.140

micro-flow channels for fuel and oxidant input and the MEA are fabricated entirely in a Nafion membrane. Nafion is the most widely used membrane in fuels cells that utilize a polymer electrolyte. This is due to its mechanical stability, superior conductivity, and permeation selectivity. The fabrication process leverages electron beam lithography for high-precision pattern creation, and dry etching for pattern transfer and aspect ratio manipulation. This new design can result in the use of fewer materials for the deployment of a compact, low weight, high energy density power source.

2. Experiment

2.1. MEA fabrication process

Nafion 212 membranes purchased from fuelcellsotre.com were used in this work. Fig. 1 illustrates the standard fabrication procedure employed. In preparation for the microfabrication process, Nafion 212 is mounted on a silicon wafer using Kapton tape. A 30 nm germanium (Ge) layer is sputter deposited using a Lesker PVD-75 sputter coater equipped with a thickness monitor for film thickness and rate determination. Zep 520A electron beam resist was subsequently spun and baked. The substrate was then exposed using a JEOL 6300FS electron beam system. The nominal dose and current were 150 μC cm^{-2} and 15 nA respectively. Following exposure, the substrate was developed in xylene and then dried using a nitrogen gun. The developed structure was first etched in CHF_3 gas to transfer the developed pattern into the Ge mask, followed by O_2 etching for pattern transfer into Nafion. After the required pattern depth is achieved via O_2 etching, a terminal CHF_3 etching step is performed to remove residual Ge. The resulting structure is shown in Fig. 1b. Additional details on the patterning of Nafion using electron beam lithography can be found in Ref. [15].

In preparation for the selective deposition of the patterned electrocatalyst layer, a thin strip (∼300 μm width) of adhesive Kapton tape is aligned using an optical microscope onto the ridge separating the microchannels shown in Fig. 1b. This step is employed to prevent material deposition under the mask that may lead to electronic short circuit. A Mylar shadow mask is then placed atop this structure for selective electrode deposition. The resulting structure is shown in Fig. 1c. During the fabrication process, a combination of profilometry (Veeco Dektak 150 surface profilometer), optical microscopy (Nikon Optical Microscope), and SEM imaging (Hitachi S4800 Field emission SEM) were used for pattern verification. An SEM micrograph of the flow channels and optical image of the in-membrane μFC are shown Fig. 2a and b. For compression tests, 1000 μm × 4000 μm rectangular patterns were fabricated in Nafion and etched to a depth of 10 μm. The squares were hot-pressed at different loads, and the change in etch depth was measured via profilometry.

2.2. Fuel cell construction

The in-membrane μFC consists of two channels separated by a ridge. The channels have a width of 100 μm and are 1×10^4 μm long. The channels are connected to larger rectangular channels that serve as feed input and output ports. Each channel is etched to a depth of 10 μm, which is approximately 20% of the total thickness of Nafion 212. The separation distance between the two channels, called the ridge distance is ∼400 μm. The ridge distance is the shortest distance for proton transport in the microfabricated μFC.

Conventional Pt/C dispersion and sputtered Pt were deposited as catalyst layers in this work. Pt (15 nm) sputtering was done using a Lesker PVD-75 sputter coater. The gas pressure, power and deposition rate were 5 mTorr, 70 W, 0.08 nm s^{-1} respectively. Pt/C was deposited by spraying a sonicated mixture of 50% Pt on carbon dispersed in isopropanol/water/ionomer mixture onto the masked patterned membrane with a spray gun. The carbon to ionomer ratio was 1.2 to 1. The Pt/C layer was ∼1 μm thick based on profilometer measurements of the catalyst deposited outside the channel. However, the catalyst layer is likely thicker within the channel due to the leveling effect of the sprayed-on liquid mixture before curing. Fig. 2c shows a top-view image of the in-membrane μFC with sputter deposited Pt. It is evident that the catalyst/electrode was not deposited in the masked center line which appears lighter in the image. The area adjacent to the ridge (0.001 cm^2) is used as the active area in our calculations. In conventional fuel cells that use sputter deposited Pt as catalyst layer, layer thickness and substrate roughness are important considerations, as film continuity can limit access to the reaction zone [16,17]. Given the roughness present in the IMFC (Fig. 1a), a 15 nm was used in this work.

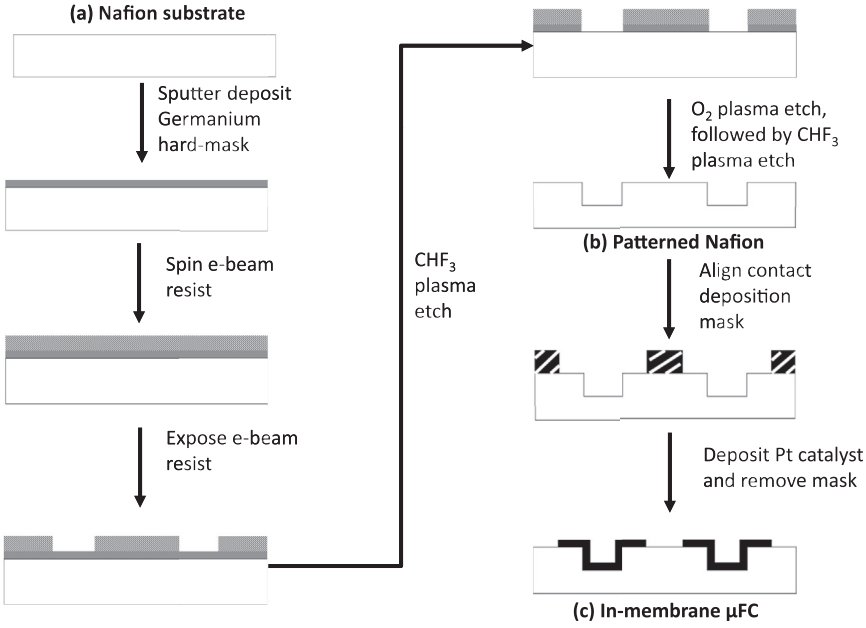

Fig. 1. Flow diagram for the fabrication of the in-membrane μFC.

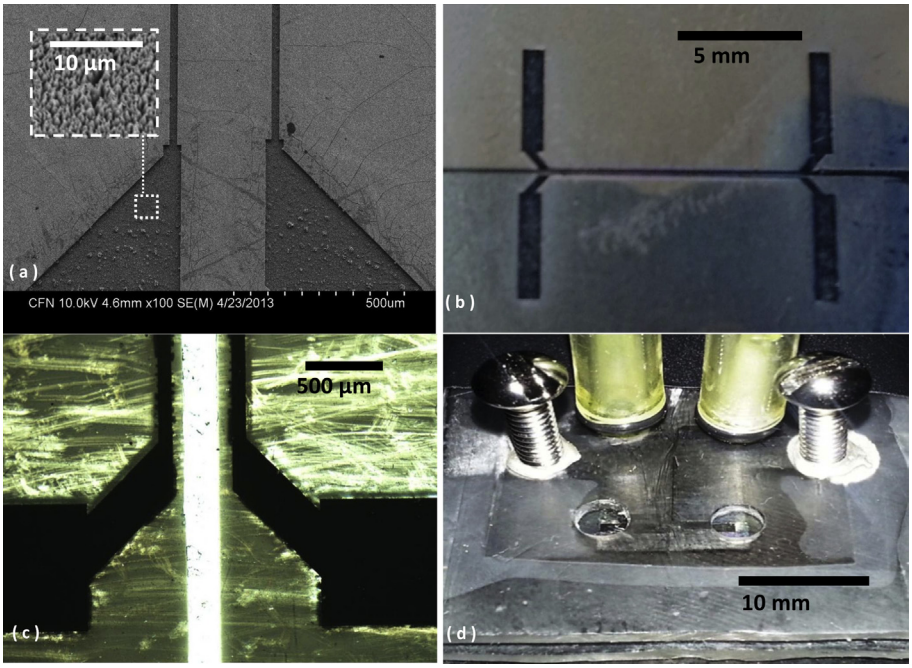

Fig. 2. (a) SEM image of channels fabricated in Nafion with 15 nm sputter deposited Pt and inset image showing channel roughness. Optical images of (b) full-length in-membrane µFC, (c) µFC after selective electrode deposition, and (d) fully assembled µFC test fixture.

A fixture made from 1.5 mm thick acrylic plastic was constructed for mounting the in-membrane µFC for testing. Two sheets of 4 cm × 4 cm acrylic plastic sheets were selected to form the top and the bottom structures encasing the µFC. A total of six holes were drilled into the top structure, including four holes to serve as anode and cathode inlet and outlets, and two holes to make room for electrical connection. The microfabricated cell is sandwiched between the two plastic sheets, with inlet and outlet holes aligned to those on the µFC. This structure is hot-pressed at 135 °C and ∼300 lbs for 20 s using a Carver model 4388 hot-press equipped with digital pressure gauge. Upon removal from the hot-press, the substrate is placed on a flat surface and lightly pressed as it cools. A set of screws is then glued into the holes for electrical connection using conductive silver epoxy as binder. The assembled fixture is shown in Fig. 2d.

2.3. Electrochemical characterization

A Scribner 850e test system equipped with humidifier bypass was used for flow rate and humidification control. For performance testing, H_2 and O_2 were fed at 20 sccm and 40 sccm to the anode and the cathode respectively. No additional backpressure was added and all testing was conducted at room temperature. The test system was set to humidifier by-pass mode during performance testing under dry conditions. Performance and impedance characterization studies were performed using a PAR 2273 potentiostat. Prior to performance testing, the test cell was conditioned at 0.3–0.4 V until the current stabilizes. During impedance testing, the frequency was scanned from 100 mHz to 100 kHz with signal amplitude of 10 mV rms. For performance testing, the cell potential was scanned in the direction of decreasing voltage.

3. Results

3.1. Effect of hotpressing on channel compression

A key concern with the procedure for making the test fixture is the compression of the microchannels during the hot-pressing procedure. Fig. 3 shows the effect of hot-press load on the compression of the rectangular patterns fabricated in Nafion. The figure shows increasing pattern compression as the load increases. At the compressive load used for making the test fixture, a 20–40% compression is observed. During the fabrication of the test fixture, the microfabricated Nafion membrane is sandwiched between two acrylic plastic sheets. Measurements of disassembled actual test cells showed a 5–10% compression for the microchannels.

3.2. Performance of in-membrane µFC

Fig. 4a shows the polarization curves for the in-membrane µFCs configured with sputtered Pt and conventional Pt/C catalyst layers under humidified and dry testing conditions. The plot shows a reduced OCV of ∼0.65 V for both the sputtered and conventional cells under dry conditions, in comparison to ∼0.92 V under humidified conditions. This difference is indicative of significant gas crossover during testing under dry conditions likely by gas permeation at the sealing interfaces [4]. Under humidified conditions, H_2O condensation, and swelling of the membrane to better

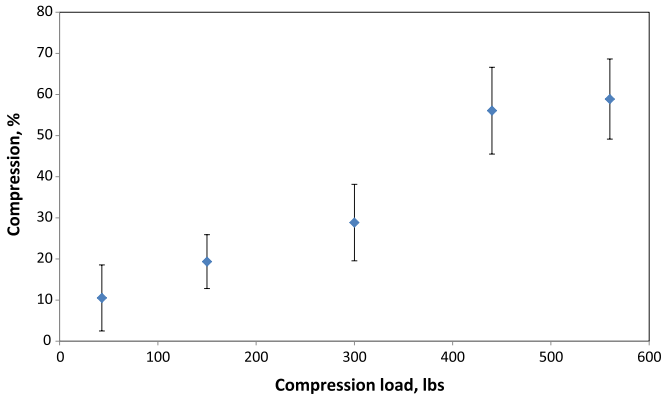

Fig. 3. Compressibility of micropatterns from hot-pressing.

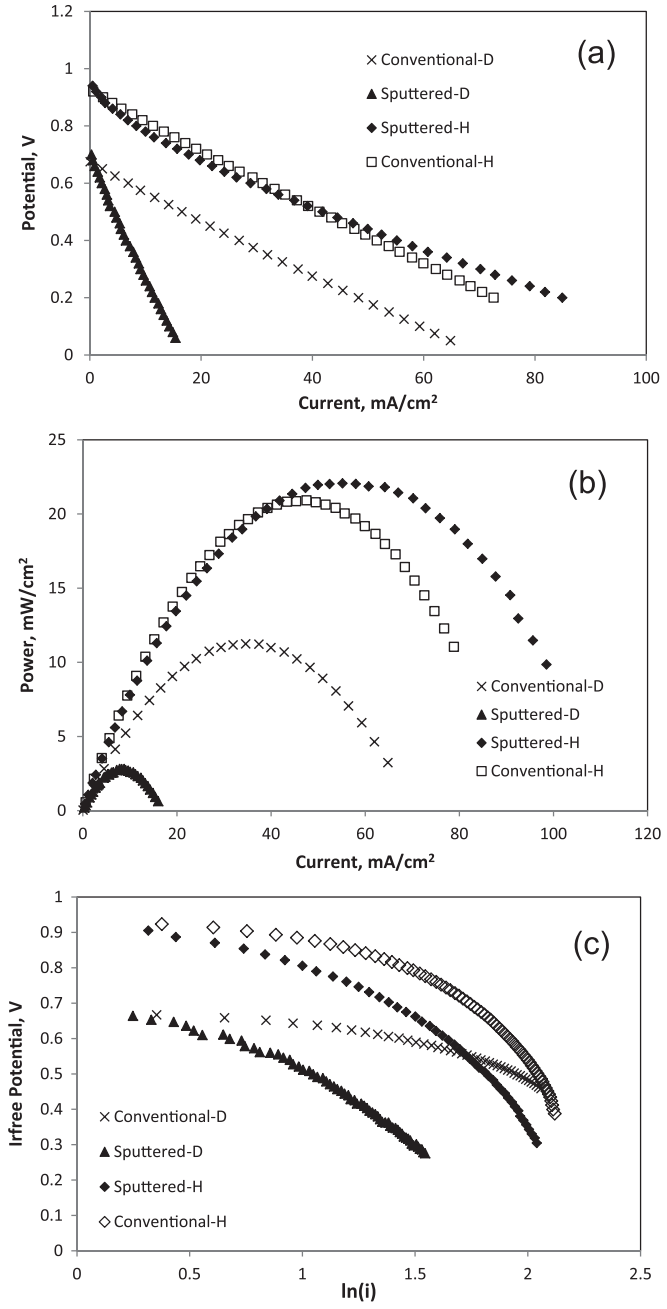

Fig. 4. (a) Polarization, (b) Power and (c) Tafel curves for the in-membrane μFC under humidified (H) and dry (D) conditions.

contact the top sealing plate can mitigate gas crossover by reducing the volume available for crossover and providing a tighter seal. In the ohmic region, the plot shows similar slope for the conventional catalyst μFCs under humidified and dry, but very different slopes for the dry and humidified sputtered Pt μFCs. In comparison to the dry Pt/C μFC, the sputtered Pt cell is exposed to further dehumidification while sitting in vacuum for several hours during the sputtering process, and as such will exhibit higher resistance. The ohmic resistances determined from EIS measurements were 7.5 and 5.9 Ω-cm^2, for the dry and humidified conventional catalyst based μFCs and 25.0 and 2.6 Ω-cm^2 for the dry and humidified sputtered catalyst based μFCs. In comparison to conventional H_2 based fuel cells, these resistances are high. The likeliest contributor is electrical resistance in the in-membrane μFC results from thin electrodes serving as current collectors. In traditional fuel cells, electrical resistance is mitigated by the conductive gas diffusion layer and its adjacent bipolar plates.

The corresponding power curves to Fig. 4a are shown in Fig. 4b. The humidified sputtered cell exhibited the best performance of the four cells, while its dry counterpart exhibited the worst performance. The maximum power densities for the tested cells were 11.2 and 20.8 mW cm^{-2} for the dry and humidified conventional catalyst based μFCs and 3.0 and 22.1 mW cm^{-2} for the dry and humidified sputtered catalyst μFCs. These results trend with the observed ohmic loss.

Fig. 4c shows the corresponding Tafel plot for the in-membrane μFCs. It is apparent from the plot that the cells show similar Tafel slopes regardless of humidification, i.e., the dry and humidified sputtered cells have a similar slope and likewise the dry and humidified conventional cell have a similar slope. The plot also shows that the conventional cells have a lower slope which is indicative of a smaller sacrificed potential as current is drawn in the activation domain. The values for the Tafel slope were 63.1 and 68.3 mV dec^{-1} for the dry and humidified Pt/C μFC and 128.0 and 110.4 mV dec^{-1} for the dry and humidified sputtered Pt cells.

The benefit of humidification to performance is also more pronounced in the sputtered cell (Fig. 4b). In addition to the apparent ohmic effects, changes in concentration polarization effects may also be important. By considering the tail-end (higher current range) of the IR-freeTafel plot (Fig. 4c), the concentration polarization effects appear to be more significant for the Pt/C based μFC. In conventional PEMFC designs, the size, shape and configuration (parallel, serpentine, interdigitated) of the flow channels are important considerations for promoting flow uniformity and mitigating water management issues [18–20]. In our current investigation, the single channels with 10 × 100 μm^2 cross-sectional are to some extent capable of mitigating transport losses as shown in Fig. 4a. However, for scaling up to a multi-channel device, channel geometry optimization would be required.

4. Conclusion

We have fabricated and tested a planar μFC design where the flow channels and catalyst layers are fabricated entirely in a Nafion membrane. Experimental test cells were made by hot-pressing Nafion in an acrylic plastic sandwich. Sputtered Pt and conventional Pt/C were used as catalyst layers, and cells were tested under dry and humidified conditions. The dry μFCs exhibited crossover effects which can be mitigated by optimizing operating conditions like relative humidity. The sputtered cell had the best overall performance, and at present, its performance is limited by the significant ohmic resistance. Once fully developed to incorporate fabrications steps for feature size and ridge manipulation, and planar stacking, this new architecture can lead to the deployment of an ultra-low weight, high energy power source.

Acknowledgments

The authors are grateful to Drs. Aaron Stein, Ming Lu, and Fernando Camino for their help with the lithographic tools at Brookhaven National Laboratory (BNL). The fabrication work was performed at the Center for Functional Nanomaterials, BNL, which is supported by the U.S Department of Energy, Office of Basic Energy Sciences under contract No. DAC0298CH10886. The authors are grateful for the support of the Army Research Office under Grant No. W911NF1010453.

References

[1] J.D. Morse, Int. J. Energy Res. 31 (2007) 576–602.
[2] T. Pichonat, B. Gauthier-Manuel, Microsys. Technol. 13 (2007) 1671–1678.

[3] K. Shah, W.C. Shin, R.S. Besser, J. Power Sources 123 (2003) 172–181.
[4] Z. Xiao, C. Feng, P.C.H. Chan, I.M. Hsing, Sens. Actuators B Chem. 132 (2008) 576–586.
[5] Y. Zhang, J. Lu, H. Zhou, T. Itoh, R. Maeda, J. Microelectromech. Syst. 17 (2008) 1020–1028.
[6] S.K. Kamarudin, W.R.W. Daud, S.L. Ho, U.A. Hasran, J. Power Sources 163 (2007) 743–754.
[7] S.H. Chan, N.-T. Nguyen, Z. Xia, Z. Wu, J. Micromech. Microeng. 15 (2005) 231.
[8] N. Hashim, S.K. Kamarudin, W.R.W. Daud, Int. J. Hydrogen Energy 34 (2009) 8263–8269.
[9] K. Shah, W.C. Shin, R.S. Besser, Sens. Actuators B Chem. 97 (2004) 157–167.
[10] S.J. Lee, A. Chang-Chien, S.W. Cha, R. O'Hayre, Y.I. Park, Y. Saito, F.B. Prinz, J. Power Sources 112 (2002) 410–418.
[11] K. Gruber, H. Loibl, T. Schlauf, J. Pallanits, C. Gornik, H. Kronberger, G. Fafilek, G. Nauer, Electrochem. Commun. 9 (2007) 1288–1292.
[12] P.O. Lopez-Montesinos, N. Yossakda, A. Schmidt, F.R. Brushett, W.E. Pelton, P.J.A. Kenis, J. Power Sources 196 (2011) 4638–4645.
[13] Y.A. Song, C. Batista, R. Sarpeshkar, J. Han, J. Power Sources 183 (2008) 674–677.
[14] E.R. Choban, L.J. Markoski, A. Wieckowski, P.J.A. Kenis, J. Power Sources 128 (2004) 54–60.
[15] A. Omosebi, R.S. Besser, J. Electrochem. Soc. 158 (2011) D603–D610.
[16] R. O'Hayre, S.J. Lee, S.W. Cha, F.B. Prinz, J. Power Sources 109 (2002) 483–493.
[17] A.T. Haug, R.E. White, J.W. Weidner, W. Huang, S. Shi, T. Stoner, N. Rana, J. Electrochem. Soc. 149 (2002) A280–A287.
[18] S.-W. Cha, R. OHayre, S.J. Lee, Y. Saito, F.B. Prinz, J. Electrochem. Soc. 151 (2004) A1856–A1864.
[19] A. Aiyejina, M.K.S. Sastry, J. Fuel Cell Sci. Technol. 9 (2012) 0110111–0110124, art. no. 011011.
[20] X. Liu, H. Guo, C. Ma, J. Power Sources 156 (2006) 267–280.